Non-collocated boundary control for contact-force control of a one-link flexible arm [*]

Kaiyo Yamaguchi[a], Takahiro Endo[a,*], Yuta Kawai[a], Fumitoshi Matsuno[a]

[a]*Dept. of Mechanical Engineering and Science, Kyoto University, Kyoto, Japan*

Abstract

This paper deals with contact-force control of a one-link flexible arm whose tip is constrained to a rigid environment. To realize the contact-force control, a boundary controller is proposed based on a dynamic model represented by an infinite dimensional model. In particular, the proposed controller does not need the physical parameters in its implementation, and this results in the non-collocated boundary controller. The closed-loop system is analyzed in an appropriate Hilbert space, and it is shown that the exponential stability of the closed-loop system is obtained by setting the feedback gains to locate the eigenvalues of the closed-loop system on the complex left half-plane. In addition, in an attempt to realize the better control performance, another controller which is a modified version of our controller is proposed. Finally, the stability, robustness to the uncertainty in physical parameters, and disturbance response of the closed-loop system are investigated by numerical simulations.

Keywords: Flexible arm, contact-force control, non-collocated boundary control

1. Introduction

A flexible arm is used in various fields because of its low energy consumption and a small moment of inertia. For example, the use of a robotic arm with the small moment of inertia is desired in the medical field from the safety points of view [1], and the use of lightweight arms for reducing the energy consumption
5 is expected in the industrial field [2]. Further, in the field of bio- and nano-technologies, the flexible arm is used for holding a small object [3], and the flexible lever is utilized for measuring the surface shape of a microscopic object [4]. At these points, the flexible arm has many advantages over the rigid arm. However, the flexible arm raises undesirable vibration due to the low rigidity of the arm, and this leads to the positional accuracy problem. The equation of motion of the flexible arm is a partial differential equation (PDE), and
10 many types of research have focused on vibration control of the flexible arm modeled by PDE [5–14].

To allow a flexible arm to perform complicated tasks such as gripping an object and constructing a large space structure, it is necessary to control the contact-force between the arm and the object as well as the vibration/position control of the flexible arm. Therefore, some researches have discussed the contact-force control of a flexible arm to carry out such tasks [15–23].
15 Epponger and Seering suggested that the link flexibility leads to instability of the system under the contact-force control in [17], and this assumption was verified in [18] through the stability analysis of a flexible arm modeled by finite dimensional approximated model. Since then, several controllers have been proposed for the contact-force control problem of flexible arms based on the finite-dimensional model [19, 20]. However, the finite dimensional model might lead to spillover instability because the model neglects the
20 infinite modes. In addition, the dimensions of the controller increase with increasing numbers of the modes

---

which are considered in the controller design model, and thus the controller tends to be complicated. From these points of view, some researches have discussed the contact-force control problem of the flexible arm using an infinite dimensional setting. For example, F. Ching et al. and F. Matsuno et al. used an infinite dimensional model and they proposed controllers that asymptotically stabilize the closed-loop system [21, 22]. Further, T. Endo et al. proposed a controller for the contact-force control of the flexible arm, and they proved the exponential stability of the closed-loop system [23]. However, these controllers use the physical parameters such as length and flexural rigidity of flexible arm in the implementation of the controller, and thus these controllers could not realize the desired contact-force when there is uncertainty/deviation in the physical parameters.

To solve this problem, we propose a controller that does not need the physical parameters in its implementation. Although some previous studies have considered robust control based on infinite-dimensional models [24, 25], the proposed controllers have required the observer [24] or the full state feedback [25]. On the other hand, our proposed controllers do not need the physical parameters in the implementation of the controller, and thus our controllers are robust against the physical parameter uncertainty without the need for observers or full state feedback. Besides, there seems to be no work dealing with robust control in the force control problem of flexible arms based on the infinite-dimensional settings as in this paper. In particular, we construct the controller by the sensor feedback of the force sensor installed at the arm-tip and the damping term, and this results in the non-collocated boundary controller because of the non-collocation of contact-force sensing and motor actuation. Some works proposed collocated boundary controller for the vibration control of the flexible structures based on the infinite-dimensional model [25–27]. On the other hand, some previous researches proposed non-collocated boundary controller for the position or vibration control of a flexible structure based on an infinite dimensional setting [28–33], and L.-Y. Liu et al. proposed a non-collocated controller for the contact-force control of a flexible arm [34]. However, to the best of our knowledge, there has no non-collocated boundary controller, which exponentially stabilizes the system for the contact-force control of flexible arm based on the infinite dimensional settings. It is better to construct an exponentially stabilizing controller with regard to its control performance.

In this research, we discuss the contact-force control of a one-link flexible arm based on the infinite dimensional model. To realize the controller that does not need the physical parameters in the implementation of the controller, we propose the non-collocated boundary controller consisting of the sensor feedback of the force sensor and the damping term. Thus, even if there is uncertainty/derivation in the physical parameters, we can output the target force, unlike the previous research [23]. Then, we analyze the eigenvalue of the closed-loop system, and we show that the exponential stability of the closed-loop system can be obtained by designing appropriate feedback gains. Further, we obtain the range of feedback gains that makes the system exponentially stable. It is well known for the non-collocated controller that the large feedback gain makes the closed-loop system unstable, and we need to set feedback gains appropriately. In addition, in an attempt to realize the better control performance, we propose another controller which is a modified version of our controller. Finally, we investigate the stability, the robustness to uncertainty in physical parameters, and disturbance response of the closed-loop system by numerical simulations. The preliminary version of this paper has been published [35]. This extended version contains a new controller which is a modified version of our controller. This modified controller is proposed for getting better control performance than our controller, and the exponential stability of the closed-loop system is analyzed by the eigenvalues of the closed-loop system. In addition, this paper contains new simulation results containing the analysis of root locus of the closed-loop system and the disturbance responses.

The contributions of this paper are summarized as follows. First of all, we can point out of the following two points as the features of this paper: (i) The contact-force is controlled by flexible arm based on the infinite-dimensional model, and (ii) the exponential stability of the closed-loop system is proved theoretically. These features have also been achieved in previous studies [23]. However, in addition to these features, this paper has the following feature: (iii) the proposed controllers can output the target force even if there is uncertainty/derivation in the physical parameters, that is the controllers are robust against the uncertainty in physical parameters. The feature (iii) has not been realized in [23]. The research with the features (i)–(iii) is a novel study. Besides, to realize the feature (iii), we construct the non-collocated boundary controller.

The rest of the paper is organized as follows. The controlled system is presented in Section 2. Section 3

proposes a boundary controller and proves the exponential stability. The modified controller is proposed in Section 4. The numerical simulation results are presented in Section 5. Finally, Section 6 contains our conclusions.

2. Controlled System

2.1. System description
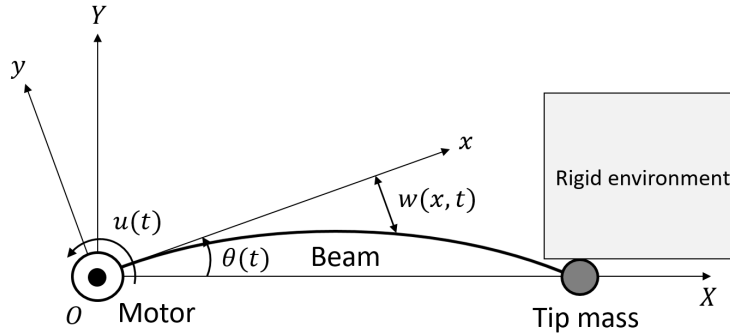
Figure 1: A flexible arm making contact with a rigid environment.

A controlled system is shown in Fig. 1. In this figure, $O - XY$ is an absolute coordinate system, and $O - xy$ is a local coordinate system that rotates with the control motor. The flexible arm is clamped to the control motor, and the tip of the arm is constrained to a surface of a rigid environment. Thus, the flexible arm is rotated in the direction of the arrow in Fig. 1 by the control motor, with the tip fixed to the environment in the Y-axis direction as shown in Fig. 1. Here, note that the tip of the flexible arm is not fixed in the X-axis direction. Let $\theta(t)$ and $\tau(t)$ be the rotation angle and the torque of the motor, respectively. Let $w(x, t)$ be the transverse displacement of the flexible arm at the position x and the time t, and $w(x, t)$ is positive in the y-axis positive direction. The flexible arm, with linear density ρ, flexural rigidity EI, and length L, satisfies the Euler-Bernoulli beam hypothesis, and $w(x, t)$ and $\theta(t)$ are assumed to be small.

The tip mass is contacted with the surface of the rigid environment, and thus the following geometric constraint is obtained:

$$\psi(t) := w(L, t) + L\theta(t) = 0. \tag{1}$$

To obtain the equations of motion of the controlled system, we derive the kinetic energy $K(t)$, the potential energy $P(t)$, and the virtual work $\delta W(t)$. Let $f(t)$ be a Lagrange multiplier associated with the constraint (1). Then, Hamilton's principle and the Lagrange multiplier gives $\int_{t_1}^{t_2} \delta(K(t) - P(t) + W(t) - f(t)\psi(t)) \mathrm{d}t = 0$, where δ is a variation, and t_1 and t_2 are time. By simple calculations, the following equations of motion are obtained as shown in [23]:

$$\begin{cases} \rho \left[w_{tt}(x, t) + xu(t) \right] + EI w_{xxxx}(x, t) = 0, & (x, t) \in (0, L) \times \mathbb{R}, \\ w(0, t) = w_x(0, t) = w_{xx}(L, t) = 0, \\ EI w_{xxx}(L, t) = f(t), \end{cases} \tag{2}$$

where Lagrange multiplier $f(t)$ is the contact-force at the tip to the surface of the environment. The contact-force $f(t)$ is the force that the flexible arm applies to the environment. The subscripts x and t denote the partial derivative with respect to the position x and the time t, respectively. The first equation in (2) describes the bending vibration of the flexible arm and others represent the boundary conditions. Here, we consider the acceleration of the control motor as the control input as shown in [5, 20], that is $\ddot{\theta}(t) = u(t)$.

The assumptions used in the controlled system are summarized as follows.

3

Assumption 1. *We assumed that $w(x,t)$ and $\theta(t)$ are small, and the flexible arm satisfies the Euler-Bernoulli beam hypothesis. In addition, the control input $u(t)$ to the system is the acceleration of the motor, $\ddot{\theta}(t) = u(t)$.*

In this paper, the flexible arm consists of a beam. The beam is assumed to be made of metal and has high rigidity, and thus we assumed that $w(x,t)$ is small. When such beam is used, we can consider that the transverse displacement $w(x,t)$ is small with respect to the length of the beam. Since $w(x,t)$ is small, the rotational angle of the motor $\theta(t)$ can be considered to be small due to the geometrical condition (1). On the other hand, we assumed that the control input $u(t)$ to the system is the acceleration of the motor, $\ddot{\theta}(t) = u(t)$. This can be realized by using the speed reference-type servo amplifier of the motor. For the implementation of the controller using the speed reference-type servo amplifier of the motor, see [5, 20] for more details.

2.2. Error system

Let $w^d(x)$ be the value of $w(x,t)$ at the equilibrium point satisfying $f(t) = f^d$. Then, $w^d(x)$ is derived as

$$w^d(x) = \frac{f^d}{6EI} x^2 (x - 3L), \tag{3}$$

where f^d is the desired contact-force and is a constant. Here, we introduce the following new variables:

$$\begin{cases} f^e(t) = f(t) - f^d, \\ w^e(x,t) = w(x,t) - w^d(x). \end{cases} \tag{4}$$

Further, we introduce the following variable transformations to eliminate $xu(t)$ in the first equation of (2):

$$L - x = x, \quad w^e(x,t) = \int_0^x \int_0^s y(L - s_1, t) \mathrm{d}s_1 \mathrm{d}s. \tag{5}$$

By applying (1), (4), and (5), the equations of motion (2) can be rewritten as follows:

$$\begin{cases} \rho y_{tt}(x,t) + EI y_{xxxx}(x,t) = 0, & (x,t) \in (0,L) \times \mathbb{R}, \\ y(0,t) = y_{xx}(0,t) = y_{xx}(L,t) = 0, \\ EI y_{xxx}(L,t) = \rho u(t), \end{cases} \tag{6}$$

and the following algebraic relation:

$$EI y_x(0,t) = -f^e(t). \tag{7}$$

3. Contact-Force Control

3.1. Controller design

The control objective of the contact-force control is to propose a controller satisfying

$$f(t) \to f^d. \tag{8}$$

Further, in this paper, we propose a controller satisfying the following conditions 1) and 2).

1) The controller is robust against uncertainty in physical parameters.
2) The closed-loop system under the proposed controller can be exponentially stable.

4

To meet these requirements, we propose the following boundary controller:

$$u(t) = -\frac{k_p}{\rho} \left[f(t) - f^d \right] + \frac{k_d}{\rho} EI w_{xxt}(0,t), \tag{9}$$

where feedback gains k_p and k_d are any positive constants. Here, note that the control objective does not include the control of the X-axis tip position of the flexible arm. Thus, our proposed controllers (9) and (48), described later, do not have the position control term. Now, we introduce constants k_p' and k_d' satisfying $k_p' = -\frac{k_p}{\rho}$ and $k_d' = \frac{EI}{\rho} k_d$. Since k_p and k_d are any positive constants, and thus k_p' and k_d' are any positive constants too. Then, the boundary controller (9) is rewritten as follows:

$$u(t) = k_p' \left[f(t) - f^d \right] + k_d' w_{xxt}(0,t). \tag{10}$$

The controller consists of two terms. The first term is the feedback of the tip force to achieve the control objective (8). The second term is the time derivative of strain at the root of the flexible arm to satisfy the condition 2). In addition, we can measure the tip force by the force sensor. The strain at the root of the beam can be measured by the strain gauge. Therefore, we do not need to use physical parameters in the implementation of the controller. Even if there is a deviation in the physical parameters such as the length and flexural rigidity of the arm, we can achieve the control objective (8), and the controller satisfies the condition 1). On the other hand, the force sensor is attached on the tip of the beam, and the motor is mounted on the root of the beam. This results in the non-collocated boundary controller because of the non-collocation of sensing and actuation. Thus, the closed-loop system in this research is non-collocated. Here, note that we assume that the speed reference-type servo amplifier of the motor is used to implement the controller as shown in [5, 20]. Thus, the speed reference voltage for the amplifier of the motor $V_{ref}(t)$ is given by

$$V_{ref}(t) = k_m \dot{\theta}(t), \tag{11}$$

where k_m is a constant gain of the servo amplifier. By setting $\dot{\theta}(0) = 0$, the controller (10) can be rewritten as

$$V_{ref}(t) = k_m k_p' \int_0^t \left[f(s) - f^d \right] \mathrm{d}s + k_m k_d' w_{xx}(0,t). \tag{12}$$

Substituting (12) into (11) yields $\ddot{\theta}(t) = k_p' \left[f(t) - f^d \right] + k_d' w_{xxt}(0,t)$, and thus we can implement the controller (10) by using the speed reference-type servo amplifier of the motor. As we mentioned earlier, we can measure the tip force and the strain at the root of the arm by the force sensor and the strain gauge, respectively. Therefore, we can easily implement the controller without the use of physical parameters. For more details of the speed reference-type servo amplifier of the motor, see [5, 20].

3.2. Closed-loop system

As the state space, the following functional space is introduced:

$$\mathbb{H} = \left\{ z = (u,v) \in H^2(0,L) \times L^2(0,L) \mid u(0) = 0 \right\}, \tag{13}$$

where the space $H^m(0,L)$ and $L^2(0,L)$ are the Sobolev space of order m and the usual square-integrable functional space, respectively. The space $\mathbb{H}$ becomes a Hilbert space with the following inner product:

$$\langle z, \hat{z} \rangle_{\mathbb{H}} = \frac{\rho}{2} \int_0^L v\bar{\hat{v}} \mathrm{d}x + \frac{EI}{2} \int_0^L u_{xx} \overline{\hat{u}_{xx}} \mathrm{d}x + \frac{1}{2} u(L) \overline{\hat{u}(L)}. \tag{14}$$

Let us define the unbounded linear operator

$$\mathbb{A} \begin{pmatrix} u \\ v \end{pmatrix} = \begin{pmatrix} v \\ -\dfrac{EI}{\rho} u_{xxxx} \end{pmatrix}, \tag{15}$$

5

with domain

$$D(\mathbb{A}) = \big\{ z = (u, v) \in H^4(0, L) \times H^2(0, L) \mid$$
$$u(0) = v(0) = u_{xx}(0) = u_{xx}(L) = 0, u_{xxx}(L) = k_p u_x(0) + k_d v(L) \big\}. \tag{16}$$

Then, the closed-loop system (6) and (9) can be written as the following evolution equation on the state space $\mathbb{H}$:

$$\frac{\mathrm{d}}{\mathrm{d}t} z(t) = \mathbb{A}z(t), \tag{17}$$

where $z(t) = (y(\cdot, t), y_t(\cdot, t))^{\mathrm{T}}$.

Now, we investigate the property of the closed-loop system.

Lemma 1. *Let $\mathbb{H}$ and $\mathbb{A}$ be defined by (13) and (15), respectively. Then, the operator $\mathbb{A}$ generates a C_0-semigroup of contractions on $\mathbb{H}$.*

PROOF. From (14)–(16), we can obtain

$$2\mathrm{Re}\langle \mathbb{A}z, z \rangle_{\mathbb{H}} = \langle \mathbb{A}z, z \rangle_{\mathbb{H}} + \langle z, \mathbb{A}z \rangle_{\mathbb{H}}$$
$$= -EIk_d|v(L)|^2 - \frac{1}{2}k_p EI u_x(0)\overline{v(L)} + \frac{1}{2}v(L)\overline{u(L)} - \frac{1}{2}k_p EI \overline{u_x(0)}v(L) + \frac{1}{2}u(L)\overline{v(L)}, \tag{18}$$

for any $z = (u, v)^{\mathrm{T}} \in D(\mathbb{A})$. By using the Cauchy-Schwarz inequality, the inequality

$$|a||b| \le 2|a||b| \le r_1|a|^2 + \frac{|b|^2}{r_2}, \qquad \text{for } a, b \in \mathbb{C}, \tag{19}$$

where r_1 and r_2 are arbitrary positive constants, and Poincaré inequality

$$\int_a^b |z(x)|^2 \mathrm{d}x \le d\left[\int_a^b |z_x(x)|^2 \mathrm{d}x + \left\{\int_a^b z(x)\mathrm{d}x\right\}^2\right], \quad \text{for } z \in H^1(a, b), \tag{20}$$

where d is a positive constant, we obtain the following inequalities:

$$\begin{cases} -u_x(0)\overline{v(L)} \le \dfrac{r_1}{2}|u_x(0)|^2 + \dfrac{1}{2r_1}|v(L)|^2, & v(L)\overline{u(L)} \le \dfrac{r_2}{2}|v(L)|^2 + \dfrac{1}{2r_2}|u(L)|^2, \\[2mm] -\overline{u_x(0)}v(L) \le \dfrac{r_1}{2}|u_x(0)|^2 + \dfrac{1}{2r_1}|v(L)|^2, & u(L)\overline{v(L)} \le \dfrac{r_2}{2}|u(L)|^2 + \dfrac{1}{2r_2}|v(L)|^2, \\[2mm] |u_x(0)|^2 \le 2(1+d)\displaystyle\int_0^L |u_{xx}|^2 \mathrm{d}x + 2d|u(L)|^2. \end{cases} \tag{21}$$

From (18) and (21), the estimate (18) yields

$$\mathrm{Re}\langle \mathbb{A}z, z \rangle_{\mathbb{H}} \le -\frac{1}{2}\left(EIk_d - \frac{EI}{2r_1}k_p - \frac{1}{2r_2}\right)|v(L)|^2 + \frac{1}{2}k_p EI r_1(1+d)\int_0^L |u_{xx}|^2 \mathrm{d}x$$
$$+ \left(\frac{r_2}{4} + \frac{k_p}{2}r_1 EI d\right)|u(L)|^2$$
$$\le -\frac{1}{2}\left(EIk_d - \frac{EI}{2r_1}k_p - \frac{1}{2r_2}\right)|v(L)|^2 + \alpha\langle z, z \rangle_{\mathbb{H}}, \tag{22}$$

where

$$\alpha = \max\left\{k_p EI r_1(1+d), \frac{r_2}{2} + k_p 2r_1 EI d\right\}. \tag{23}$$

6

Thus, we obtain the following estimate from (22):

$$\mathrm{Re}\langle(\mathbb{A}-\alpha)z,z\rangle_{\mathbb{H}} \leq -\frac{1}{2}\left(EIk_d - \frac{EI}{2r_1}k_p - \frac{1}{2r_2}\right)|v(L)|^2$$
$$\leq 0, \tag{24}$$

where r_1 and r_2 are designed satisfying the following inequality:

$$EIk_d - \frac{EI}{2r_1}k_p - \frac{1}{2r_2} > 0. \tag{25}$$

Therefore, we obtain the dissipativity of the operator $(\mathbb{A}-\alpha)$.

Next, we prove that the operator $\mathbb{A}^{-1}$ is compact. A solution $z \in D(\mathbb{A})$ of $\mathbb{A}z = \hat{z}$ for any $\hat{z} = (\hat{u},\hat{v})^{\mathrm{T}} \in \mathbb{H}$ is given by

$$u(x) = c_1 x + c_2 x^3 - \frac{\rho}{EI}\int_0^x\int_0^{s_1}\int_0^{s_2}\int_0^{s_3}\hat{v}(s_4)\mathrm{d}s_4\mathrm{d}s_3\mathrm{d}s_2\mathrm{d}s_1, \tag{26}$$

$$v(x) = \hat{u}(x), \tag{27}$$

where c_1 and c_2 are the following constants:

$$\begin{bmatrix} c_1 \\ c_2 \end{bmatrix} = \begin{bmatrix} -k_p & 6 \\ 0 & 6L \end{bmatrix}^{-1}\begin{bmatrix} \frac{\rho}{EI}\int_0^L\hat{v}(s)\mathrm{d}s + k_d\hat{u}(L) \\ \frac{\rho}{EI}\int_0^L\int_0^{s_1}\hat{v}(s)\mathrm{d}s\mathrm{d}s_1 \end{bmatrix}. \tag{28}$$

Therefore, it can be seen that there are nontrivial solutions u and v, that means $\mathbb{A}^{-1}$ exists. In addition, $\mathbb{A}^{-1}$ is a compact by Sobolev's embedding theorem [36]. Furthermore, the spectrum $\sigma(\mathbb{A})$ of the operator $\mathbb{A}$ consists of isolated eigenvalues [37].

Since the spectrum $\sigma(\mathbb{A})$ consists of isolated eigenvalues, there exists a $\lambda_0 > \alpha$ such that $\lambda_0 + \alpha \in \rho(\mathbb{A})$, where $\rho(\mathbb{A}) = \mathbb{C}\setminus\sigma(\mathbb{A})$ [38]. This means that the operator $[(\lambda_0+\alpha)I - \mathbb{A}]^{-1} = (\lambda_0 I - \mathbb{A} + \alpha)^{-1}$ is bounded, and thus we obtain $\lambda_0 \in \rho(\mathbb{A}-\alpha)$. Therefore, the operator $(\mathbb{A}-\alpha)$ generates a C_0-semigroup of contractions from Lumer-Phillips theorem. In addition, the operator $\mathbb{A}$ also generates a C_0-semigroup of contractions from the perturbations by bounded linear operators [36]. $\square$

3.3. Exponential stability of the closed-loop system

First, we show the relationship between the stability of the closed-loop system and the eigenvalue of the system. Then, we show the exponential stability of the closed-loop system by analyzing the eigenvalues of the system.

3.3.1. The relationship between the stability and the eigenvalues

We analyze the asymptotic behavior of the eigenvalues of $\mathbb{A}$ to investigate the relationship between the stability and the eigenvalues. For $z = (u,v)^{\mathrm{T}} \in D(\mathbb{A})$ and eigenvalue $\lambda \in \mathbb{C}$, let us consider the eigenvalue problem $\mathbb{A}\phi = \lambda\phi$. Eliminating v in $\mathbb{A}\phi = \lambda\phi$ gives the following equations:

$$\lambda^2 u + \frac{EI}{\rho}u_{xxxx} = 0, \tag{29}$$

$$u(0) = u_{xx}(0) = u_{xx}(L) = 0, \tag{30}$$

$$u_{xxx}(L) = k_p u_x(0) + k_d\lambda u(L). \tag{31}$$

Here, note that the eigenvalue of $\mathbb{A}$ is real symmetric because of $\overline{\mathbb{A}z} = [\overline{v}, -\frac{EI}{\rho}\overline{u_{xxxx}}]^{\mathrm{T}} = \mathbb{A}\overline{z}$.

The solution of (29) can be found as

$$u(x) = C_1 e^{\beta\omega_1 x} + C_2 e^{\beta\omega_2 x} + C_3 e^{\beta\omega_3 x} + C_4 e^{\beta\omega_4 x}, \tag{32}$$

where $\lambda = \beta^2 \sqrt{\frac{EI}{\rho}}$, $\beta = |\beta|e^{i\arg\beta}$, $\omega_1 = e^{\frac{3}{4}\pi i}$, $\omega_2 = e^{\frac{\pi}{4}i}$, $\omega_3 = -\omega_2$, $\omega_4 = -\omega_1$, and the constants $C_1, \cdots, C_4$ are determined by the boundary conditions (30) and (31). From (30) and (31), the following characteristic equation is obtained:

$$\Delta(\beta) := \beta^7 \det \begin{bmatrix} 1 & 1 & 1 & 1 \\ \omega_1^2 & \omega_2^2 & \omega_3^2 & \omega_4^2 \\ W_1 & W_2 & W_3 & W_4 \\ P_1 & P_2 & P_3 & P_4 \end{bmatrix} = 0, \tag{33}$$

where

$$\begin{cases} W_i = \omega_i^2 e^{\beta\omega_i L}, \\ P_i = \omega_i^3 e^{\beta\omega_i L} - \dfrac{k_d}{\beta}\sqrt{\dfrac{EI}{\rho}}e^{\beta\omega_i L} - \dfrac{k_p}{\beta^2}\omega_i, \end{cases} \quad \text{for } i = 1, \cdots, 4. \tag{34}$$

Now, we investigate the eigenvalues of $\mathbb{A}$ on the two sectors $S = \{\beta \in \mathbb{C} : \frac{\pi}{4} \leq \arg\beta \leq \frac{\pi}{2}\}$ and $S_0 = \{\beta \in \mathbb{C} : 0 \leq \arg\beta < \frac{\pi}{4}\}$. In the following, we consider the case that $|\beta|$ is large enough, that is the eigenvalues located far from the origin of the complex plane.

First, we consider the characteristic equation on the sector S_0. In the sector S_0, it can be seen that $\mathrm{Re}(\beta\omega_1) < 0$, $\mathrm{Re}(\beta\omega_2) > 0$, $\mathrm{Re}(\beta\omega_3) < 0$, and $\mathrm{Re}(\beta\omega_4) > 0$, and thus we obtain $|e^{\beta\omega_1}| \approx 0$, $|e^{-\beta\omega_2}| \approx 0$, $|e^{\beta\omega_3}| \approx 0$, and $|e^{-\beta\omega_4}| \approx 0$. Substituting these facts into (33) gives

$$\Delta(\beta) = -\beta^7 e^{\rho(\omega_2+\omega_4)L} \det \begin{bmatrix} 1 & 0 & 1 & 0 \\ -1 & 0 & 1 & 0 \\ 0 & 1 & 0 & -1 \\ -\frac{k_p}{\beta^2}\omega_1 & i\omega_2 - \frac{k_d}{\beta}\sqrt{\frac{EI}{\rho}} & \frac{k_p}{\beta^2}\omega_2 & i\omega_1 - \frac{k_d}{\beta}\sqrt{\frac{EI}{\rho}} \end{bmatrix} = 0. \tag{35}$$

Thus, the characteristic equation on S_0 is calculated as follows:

$$\frac{4k_d}{\beta}\sqrt{\frac{EI}{\rho}} + 2\sqrt{2} \neq 0. \tag{36}$$

This means that the eigenvalue does not exist on this sector far from the origin.

Next, we consider the characteristic equation on the sector S. In this sector, by the same method as above, the characteristic equation is calculated as follows because of $\mathrm{Re}(\rho\omega_1) \approx 0$:

$$\Delta(\beta) = 2\sqrt{2}\beta^7 e^{\beta\omega_4 L}\left[\left(i + \frac{\sqrt{2}k_d}{\beta}\sqrt{\frac{EI}{\rho}}\right)e^{-\beta\omega_2 L} - \left(1 + \frac{\sqrt{2}k_d}{\beta}\sqrt{\frac{EI}{\rho}}\right)e^{\beta\omega_2 L} + \mathcal{O}(\beta^{-2})\right] = 0. \tag{37}$$

To show the operator $\mathbb{A}$ satisfies the spectrum-determined growth condition, we use the result of [39]. According to this result, if the characteristic equation represented by

$$\Delta(\beta) = \beta^7 e^{\beta\omega_4}\left([\Theta_{-1}(\beta)]_1 e^{-\rho\omega_2} + [\Theta_0(\beta)]_1 + [\Theta_1(\beta)]_1 e^{\rho\omega_2}\right) \tag{38}$$

satisfies

$$\Theta_{00}^2 - 4\Theta_{1,0}\Theta_{-1,0} \neq 0, \tag{39}$$

then the spectrum-determined growth condition holds, where $[\Theta_i(\beta)]_1 = \Theta_{i0} + \mathcal{O}(\beta^{-1})$, Θ_{i0} is constant, and $i = -1, 0, 1$. Here, note that we say that a C_0-semigroup $\mathbb{T}(t)$ generated by $\mathbb{A}$ satisfies the spectrum-determined growth condition if the growth rate $\omega_0 = \inf_{t>0} \log\|\mathbb{T}(t)\|/t$ is equal to $\sup\{\mathrm{Re}\lambda \in \sigma(\mathbb{A})\}$, where the classical solution of (17) is given by $z(t) = \mathbb{T}(t)z(0)$. It is easy to check that the characteristic equation (37) satisfies (39). Therefore, the operator $\mathbb{A}$ defined by (15) satisfies the spectrum determined growth condition [39], and the exponential stability of (17) is determined by the sign of the real parts of the eigenvalues. These are summarized as follows.

Theorem 2. *If the feedback gains are set so that the real parts of the eigenvalues are negative, the closed-loop system* (17) *is exponentially stable.*

3.3.2. Exponential stability

Now, in order to examine the exponential stability of the system (17), we investigate the sign of the real parts of eigenvalues. From the characteristic equation on the sector S (37), we obtain

$$\left(i + \frac{\sqrt{2}k_d}{\beta}\sqrt{\frac{EI}{\rho}}\right)e^{-\beta\omega_2 L} - \left(1 + \frac{\sqrt{2}k_d}{\beta}\sqrt{\frac{EI}{\rho}}\right)e^{\beta\omega_2 L} + \mathcal{O}(\beta^{-2}) = 0. \tag{40}$$

Using a Taylor series in this equation gives $e^{\beta\omega_2 L} - ie^{-\beta\omega_2 L} + \mathcal{O}(\beta^{-1}) = 0$. This equation has the following solution by virtue of Rouche's theorem: $\beta_n = \tilde{\beta}_n + \mathcal{O}(n^{-1})$, where $n \in \mathbb{N}$ and $\tilde{\beta}_n = \frac{\pi i}{\omega_2 L}(n + \frac{1}{4})$. Substituting this solution into (40) and using a Taylor series lead to $\mathcal{O}(n^{-1}) = -\frac{k_d}{\tilde{\beta}_n}\sqrt{\frac{EI}{\rho}} + \mathcal{O}(n^{-2})$. Therefore, we obtain $\beta_n = \tilde{\beta}_n - \frac{k_d}{\tilde{\beta}_n}\sqrt{\frac{EI}{\rho}} + \mathcal{O}(n^{-2})$ which results in

$$\lambda_n = -2k_d\sqrt{\frac{EI}{\rho}} + \frac{i\pi^2}{L^2}\left(n + \frac{1}{4}\right)^2 + \mathcal{O}(n^{-1}) \quad (n = 1, 2, 3\cdots), \tag{41}$$

Here, note that $1/\omega_2^2 = -i$. From this, the real parts of all eigenvalues are negative when the eigenvalues are located far from the origin.

Next, we investigate the eigenvalues in the region where the eigenvalues are located close to the origin so that it can be numerically analyzed. To determine the parameter set (k_p, k_d) of the controller such that the real parts of the eigenvalues, which are close to the origin, are negative, we use the parameter space method [40, 41]. In the first step, to obtain the boundary of the stable region in the parameter space (k_p, k_d), we derive k_p and k_d where the real parts of eigenvalues are zero. For this, let us consider the case where the eigenvalue is expressed as follows:

$$\lambda = \beta^2\sqrt{\frac{EI}{\rho}}, \qquad \text{where} \quad \beta = \sqrt{y^2 i}, \quad y \in \mathbb{R}. \tag{42}$$

Substituting (42) into (33) leads to the following characteristic equation:

$$\Delta(\beta) = g_1 + g_2 i = 0, \tag{43}$$

where

$$g_1 = -16\sqrt{\frac{EI}{\rho}}y^2 k_d \sin(yL)\sinh(yL), \tag{44}$$

$$g_2 = -8y\left\{\left[k_p + y^2\cos(yL)\right]\sinh(yL) + \left[k_p - y^2\cosh(yL)\right]\sin(yL)\right\}. \tag{45}$$

Solving (43) gives the following k_p and k_d:

(i) When $y = \frac{n\pi}{L}$:

$$k_p = \frac{n^2\pi^2}{L^2} \quad (n = 1, 3, 5\cdots), \qquad k_d = any \tag{46}$$

(ii) When $y \neq \frac{n\pi}{L}$:

$$k_p = \frac{y^2\left[\cosh(yL)\sin(yL) - \sinh(yL)\cos(yL)\right]}{\sinh(yL) + \sin(yL)}, \qquad k_d = 0. \tag{47}$$

Since the boundary of the stable region is obtained, we derive k_p and k_d where the real parts of eigenvalues are not negative by using numerical calculation software. By substituting complex number whose real parts are not negative into the characteristic equation (33), we obtain k_p and k_d so that the system has eigenvalues

9
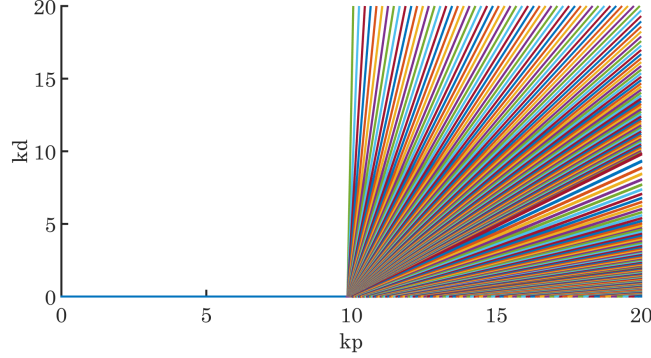
Figure 2: Unstable region under the proposed controller (9).

whose real parts are not negative. As the example, we show the k_p and k_d on the $k_p - k_d$ plane as shown in Fig. 2. All of the values of physical parameters are set as 1. In this figure, the horizontal axis represents the feedback gain k_p, and the vertical axis is the feedback gain k_d. The hatched region represents the area of feedback gains k_p and k_d having eigenvalues whose real part is positive. Here, note that we want to examine the regions of k_p and k_d where the closed-loop system is exponentially stable, that is, the eigenvalues are negative. For this reason, it may seem better to directly find k_p and k_d when the real parts of the eigenvalues are negative. However, an infinite-dimensional model has an infinite number of eigenvalues. For this reason, it is impossible to numerically obtain the feedback gains k_p and k_d in which the real parts of infinite eigenvalues are all negative. Therefore, in this paper, the stability is discussed after finding k_p and k_d where the real part is positive. In this figure, the stable region is the unhatched region. From this figure, if k_p and k_d are set as the values on the unhatched region, the real part of the eigenvalue is negative, so the system becomes exponentially stable. In other words, if $k_p < \frac{\pi^2}{L^2}$, it turns out that the system becomes exponentially stable because of theorem 2 and the facts that the real parts of eigenvalues far from the origin are negative from (41) and the real parts of eigenvalues in the region where the eigenvalues are close to the origin are negative.

Finally, we investigate the root locus of the system in order to confirm this fact. We derive some eigenvalues by the Newton Raphson method and plot them when k_p is gradually increased from 1 as shown in Fig. 3. All of the values of physical parameters and k_d are set as 1. From this figure, it can be seen that the real parts of some eigenvalues increase according to k_p. In addition, two eigenvalues near the origin cross the imaginary axis when $k_p = \frac{\pi^2}{L^2}$. And other eigenvalues do not cross the imaginary axis or cross when k_p is a value which is bigger than $\frac{\pi^2}{L^2}$. This value increases according to the distance from the origin. From these facts and theorem 2, it can be seen that when $k_p > \frac{\pi^2}{L^2}$, the real part of some eigenvalues is positive, so the system becomes unstable. Here, note that Fig. 3 is a figure to confirm the fact that the system becomes exponentially stable if $k_p < \pi^2/L^2$. From Fig. 3, we found that the reason why the closed-loop system becomes unstable when $k_p > \pi^2/L^2$ in Fig. 2 is because the real parts of the two eigenvalues near the origin in Fig. 3 become positive when $k_p > \pi^2/L^2$.

4. Modified controller design

4.1. Design of modified controller

It is known that the time derivative of the shear force at the root of the flexible arm, $w_{xxxt}(0, t)$, suppresses the vibration more than the time derivative of the strain at the root of the arm, $w_{xxt}(0, t)$ [42]. In particular, the real parts of the eigenvalues of the system under the feedback of $w_{xxxt}(0, t)$ would tend to $-\infty$ as the distance between the eigenvalues and the origin increases. On the other hand, the real parts of the eigenvalues of the system under the feedback control of $w_{xxt}(0, t)$ would tend to a vertical line
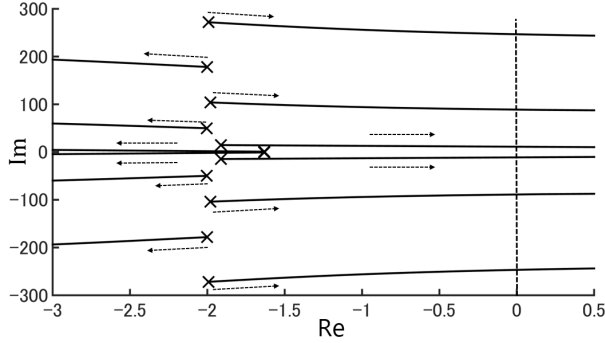
Figure 3: Root loci of the system under the proposed controller (9).

which is parallel to the imaginary axis [43]. Thus, it seems that the feedback control of $w_{xxxt}(0,t)$ can well suppress vibration of high frequency. From this fact, to realize the better control performance, we propose the following new controller:

$$u(t) = -\frac{k_p}{\rho} \left[f(t) - f^d \right] - \frac{EI}{\rho} k_d w_{xxxt}(0,t). \tag{48}$$

The first term of the controller is the feedback of the contact-force at the arm-tip to realize the control objective $(f(t) \rightarrow f_d)$. The second term is corresponding to the damping term consisting of the time derivative of the shear force at the root of the arm to suppress the vibration. Moreover, the contact-force at the tip and the shear force at the root of the beam can be measured by the force sensor and the strain gauge, respectively. To implement the controller, we use the speed reference-type servo amplifier of the motor as shown in (12). Therefore, we do not need to use the physical parameter in the implementation of this controller, and thus the controller is robust against uncertainty in physical parameters.

4.2. Closed-loop system under the modified controller

To formulate the system in the state space $\mathbb{H}$ defined by (13), let us define the linear operator

$$\mathbb{B} \begin{pmatrix} u \\ v \end{pmatrix} = \begin{pmatrix} v \\ -\dfrac{EI}{\rho} u_{xxxx} \end{pmatrix}, \tag{49}$$

with domain

$$D(\mathbb{B}) = \big\{ z = (u,v) \in H^4(0,L) \times H^2(0,L) \mid$$
$$u(0) = v(0) = u_{xx}(0) = u_{xx}(L) = 0, u_{xxx}(L) = k_p u_x(0) + k_d v_x(L) \big\}. \tag{50}$$

The difference between the operator $\mathbb{A}$ and $\mathbb{B}$ is the boundary condition in the domain. The closed-loop system (6) and (48) can be represented as the following evolution equation on $\mathbb{H}$,

$$\frac{\mathrm{d}}{\mathrm{d}t} z(t) = \mathbb{B} z(t), \tag{51}$$

where $z(t) = (y(\cdot,t), y_t(\cdot,t))^{\mathrm{T}}$.

As the property of the operator $\mathbb{B}$, we have the following lemma:

Lemma 3. *Let $\mathbb{B}$ be defined by (49). Then, $\mathbb{B}^{-1}$ exists and compact. Therefore, the spectrum of $\mathbb{B}$ consists of the isolated eigenvalues with finite multiplicities.*

PROOF. The proof is the same manner in the proof of lemma 1 and is straightforward. Thus, it is omitted.

$\square$

11

4.3. Eigenvalue analysis of $\mathbb{B}$

The feedback control of $w_{xxxt}(0,t)$ leads to the lack of the dissipativity, and we cannot show the estimation of the operator $\mathbb{B}$ like the operator $\mathbb{A}$ (24). Thus, it is difficult to show the existence of a C_0-semigroup using the estimation of the operator like (24). Here, we investigate the exponential stability and the C_0-semigroup generation from the eigenvalue analysis.

For $z = (u,v)^{\mathrm{T}} \in D(\mathbb{B})$ and the eigenvalue $\lambda' \in \mathbb{C}$, we consider the eigenvalue problem $\mathbb{B}\phi = \lambda'\phi$. Using the same procedure in section 3.3 gives the following characteristic equation:

$$\Delta(\gamma) := \gamma^7 \det \begin{bmatrix} 1 & 1 & 1 & 1 \\ \omega_1^2 & \omega_2^2 & \omega_3^2 & \omega_4^2 \\ W_1 & W_2 & W_3 & W_4 \\ P_1 & P_2 & P_3 & P_4 \end{bmatrix} = 0, \tag{52}$$

where

$$\begin{cases} W_i = \omega_i^2 \mathrm{e}^{\gamma \omega_i L}, \\ P_i = \omega_i^3 \mathrm{e}^{\gamma \omega_i L} - k_d \sqrt{\dfrac{EI}{\rho}} \omega_i \mathrm{e}^{\gamma \omega_i L} - \dfrac{k_p}{\gamma^2} \omega_i, \end{cases} \qquad \text{for } i = 1, \cdots, 4, \tag{53}$$

$\lambda' = \gamma^2 \sqrt{\frac{EI}{\rho}}$, $\gamma = |\gamma| \mathrm{e}^{i \arg \gamma}$, $\omega_1 = \mathrm{e}^{\frac{3}{4}\pi i}$, $\omega_2 = \mathrm{e}^{\frac{\pi}{4} i}$, $\omega_3 = -\omega_2$, and $\omega_4 = -\omega_1$.

We investigate the eigenvalues of $\mathbb{B}$ on the two sectors S and S_0 like section 3.3. In the following, we consider $|\gamma|$ is large enough.

The characteristic equation on the sector S_0 is obtained as follows:

$$2\sqrt{2} k_d \sqrt{\frac{EI}{\rho}} + 2\sqrt{2} \neq 0. \tag{54}$$

Thus, we found that the eigenvalues do not exist in this sector far from the origin.

On the other hand, the characteristic equation on the sector S is given by

$$\Delta(\gamma) = 2\sqrt{2} \gamma^7 \mathrm{e}^{\gamma \omega_4 L} \left[-\mathrm{e}^{\gamma \omega_2 L} \left(1 + k_d \sqrt{\frac{EI}{\rho}} \right) + i \left(1 - k_d \sqrt{\frac{EI}{\rho}} \right) \mathrm{e}^{-\gamma \omega_2 L} + \mathcal{O}(\gamma^{-2}) \right] = 0. \tag{55}$$

When $k_d = \sqrt{\frac{\rho}{EI}}$, this leads to

$$2\mathrm{e}^{\gamma \omega_2 L} + \mathcal{O}(\gamma^{-2}) \neq 0. \tag{56}$$

Therefore, when $k_d = \sqrt{\frac{\rho}{EI}}$, eigenvalue does not exist. On the other hand, when $k_d \neq \sqrt{\frac{\rho}{EI}}$, solving (55) gives the following γ_n and λ'_n:

$$\gamma_n = \frac{1}{2\omega_2 L} \ln|K| + \frac{i}{2\omega_2 L} \left(\frac{\pi}{2} + 2n\pi \right) + \mathcal{O}(n^{-2}), \tag{57}$$

$$\lambda'_n = \frac{1}{2L^2} \sqrt{\frac{EI}{\rho}} \left(\frac{\pi}{2} + 2n\pi \right) \ln|K| + \frac{i}{4L^2} \sqrt{\frac{EI}{\rho}} \left[\left(\frac{\pi}{2} + 2n\pi \right)^2 - (\ln|K|)^2 \right] + \mathcal{O}(n^{-1}), \tag{58}$$

where $K = \frac{1 - k_d\sqrt{EI/\rho}}{1 + k_d\sqrt{EI/\rho}}$, $n = 1, 2, 3 \cdots$. From $|K| = |\frac{1 - k_d\sqrt{EI/\rho}}{1 + k_d\sqrt{EI/\rho}}| < 1$, $\frac{\sqrt{EI/\rho}}{2L^2}(\frac{\pi}{2} + 2n\pi) \ln|K|$ is negative.

Therefore, we found that the real parts of all eigenvalues are negative when the eigenvalues are far from the origin. Here, the characteristic equation (55) satisfies (39) if $k_d \neq \sqrt{\frac{\rho}{EI}}$. Therefore, we found the following facts from [39]: the spectrum-determined growth condition holds, the system is exponentially stable and the operator $\mathbb{B}$ generates a C_0-semigroup if the real parts of eigenvalues are negative. To summarize, we have the following theorem:

12

Theorem 4. *Let $\mathbb{H}$ and $\mathbb{B}$ be defined by* (13) *and* (49), *respectively. If $k_d \neq \sqrt{\frac{\rho}{EI}}$ and the feedback gains are set so that the real parts of the eigenvalues are negative, the closed-loop system* (51) *is exponentially stable, and the operator $\mathbb{B}$ generates a C_0-semigroup on $\mathbb{H}$.*

We have already shown that the real parts of the eigenvalues located far from the origin are negative as shown in (58).

Next, using the same procedures in section 3.3, we consider the eigenvalues in the region where the eigenvalues are close to the origin so that it can be numerically analyzed. First, to obtain the boundary of the stable region, we investigate the eigenvalues located on the positive imaginary axis as follows:

$$\lambda' = \sqrt{\frac{EI}{\rho}}\gamma^2, \qquad \text{where} \quad \gamma = \sqrt{\kappa^2 i}, \quad \kappa \in \mathbb{R}. \tag{59}$$

Substituting (59) into (52) gives the following characteristic equation:

$$\Delta(\gamma) = f_1 + f_2 i = 0, \tag{60}$$

$$f_1 = 4\sqrt{2}\Bigg\{ -\kappa^2 \left(k_d\sqrt{\frac{EI}{\rho}} + 1 \right) \sin(\kappa L)\cosh(\kappa L)$$

$$- \kappa^2 \left(k_d\sqrt{\frac{EI}{\rho}} - 1 \right) \cos(\kappa L)\sinh(\kappa L) + k_p(\sin(\kappa L) + \sinh(\kappa L)) \Bigg\}, \tag{61}$$

$$f_2 = 4\sqrt{2}\Bigg\{ -\kappa^2 \left(k_d\sqrt{\frac{EI}{\rho}} - 1 \right) \sin(\kappa L)\cosh(\kappa L)$$

$$- \kappa^2 \left(k_d\sqrt{\frac{EI}{\rho}} + 1 \right) \cos(\kappa L)\sinh(\kappa L) - k_p(\sin(\kappa L) + \sinh(\kappa L)) \Bigg\}. \tag{62}$$

Solving (60) gives the following k_p and k_d:
(i)When κ satisfies $\sin(\kappa L)\cosh(\kappa L) + \cos(\kappa L)\sinh(\kappa L) \neq 0$

$$k_p = \frac{\kappa^2\{\sin(\kappa L)\cosh(\kappa L) - \cos(\kappa L)\sinh(\kappa L)\}}{\sin(\kappa L) + \sinh(\kappa L)}, \qquad k_d = 0. \tag{63}$$

(ii)When κ satisfies $\sin(\kappa L)\cosh(\kappa L) + \cos(\kappa L)\sinh(\kappa L) = 0$

$$k_p = \frac{2\sin(\kappa L)\cosh(\kappa L)}{\sin(\kappa L) + \sinh(\kappa L)}\kappa^2, \qquad k_d = \text{any}. \tag{64}$$

The boundary of the stable region is found, and thus we can derive k_p and k_d where the real parts of the eigenvalues become non-negative with numerical calculations. By using the same procedure in section 3.3.2, we obtain k_p and k_d so that the real parts of the eigenvalues are not negative as shown in Fig. 4. Here, all of the physical parameter values are set as 1. From this figure, it can be seen that if $k_p < 7.043$, which is derived from (64), the real parts of the eigenvalues are negative, and thus we obtain the exponential stability of the closed-loop system, and we found that the operator $\mathbb{B}$ generates a C_0-semigroup. However, we found that the stable region of the newly proposed controller is narrower than of the controller proposed in section 3. In addition, whether the newly proposed controller suppresses high-frequency vibration compared to the controller in section 3 is verified by numerical simulations in the next section.

5. Numerical Simulations

In order to conduct numerical simulations, we used the eigenfunction expansion method and derived the finite dimensional model. In the simulation, we used MATLAB/Simulink as the software, and we

13
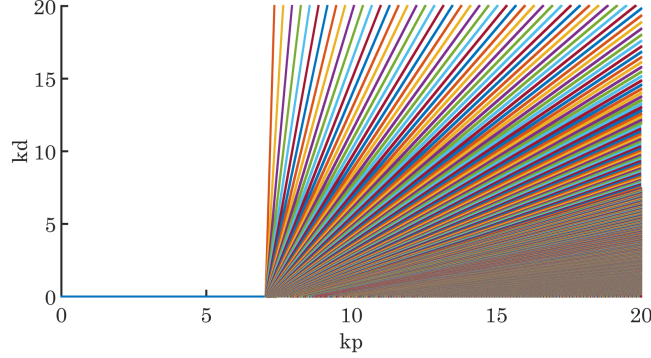
Figure 4: Unstable region under modified controller (48).
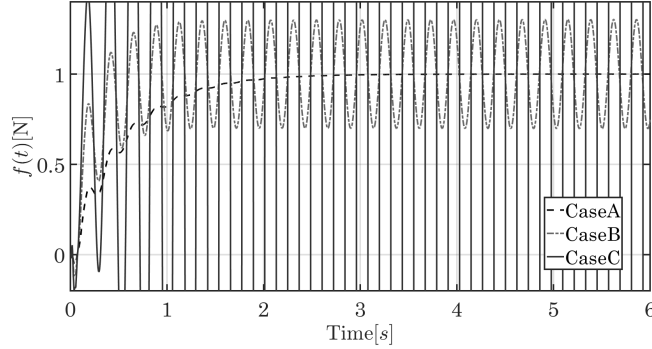
Figure 5: Contact-force $f(t)$ under the proposed controller (9).

considered first twelve modes and set the physical parameters as follows: $E = 2.06 \times 10^{11}[\mathrm{N/m^2}], I = 3.33 \times 10^{-11}[\mathrm{m^4}], L = 1.05[\mathrm{m}]$, and $\rho = 0.78[\mathrm{kg/m}]$. Here note that, if the number of modes is increased to 13 or more, the numerical error becomes large, and we could not obtain the eigenvalues. Thus, we used the first twelve modes in the numerical simulations. If more modes are required, we consider that it is necessary to make the system dimensionless.

First, to support the stable region in the section 3.3, we consider the step response of the desired contact force $f^d = 1[N]$ for the following three cases: case A: $k_p = 4(< \frac{\pi^2}{L^2}), k_d = 2$, case B: $k_p = \frac{\pi^2}{L^2}, k_d = 2$, and case C: $k_p = 15(> \frac{\pi^2}{L^2}), k_d = 2$. Here, we used our controller (9). Fig. 5 shows the step response of the contact-force. In this figure, the dashed line represents the response of case A (gain k_p is in the stable region). The contact-force $f(t)$ in case A converges to the designed value. Fig. 6 shows the transverse displacement of the beam, $w(x, t)$, in the case A. From Fig. 6, we found that the response of $w(x, t)$ has no undesired vibration and converges to the designed value.

On the other hand, the dash-dotted line and solid line in Fig. 5 represent the responses of contact-force when case B (k_p is on the boundary of the stable region) and case C (k_p is in the unstable region), respectively. When k_p is on the boundary of the stable region, the vibration occurs in the response of $f(t)$, and the response of $f(t)$ does not converge to the designed value. In addition, when k_p is in the unstable region (case C), it can be seen that $f(t)$ diverges.

In addition, we confirm the stable region of the modified controller (48) shown in the section 4 for the following three cases: case A': $k_p = 4, k_d = 2$, case B': $k_p = 6.388967$ and case C': $k_p = 15, k_d = 2$ as shown in Fig. 7. Here, $k_p = 6.388967$ is the boundary value of the stable region when $L = 1.05$. From Fig. 7, the same results as the controller (9) are obtained.

14
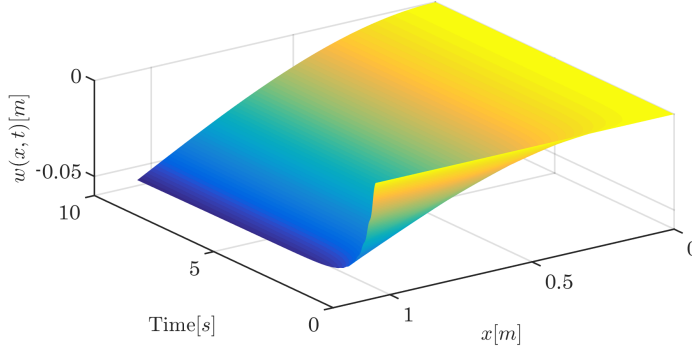
Figure 6: Transverse displacement $w(x,t)$ under the proposed controller (9) $\quad(k_p = 4, k_d = 2, \text{time} = 10s)$.
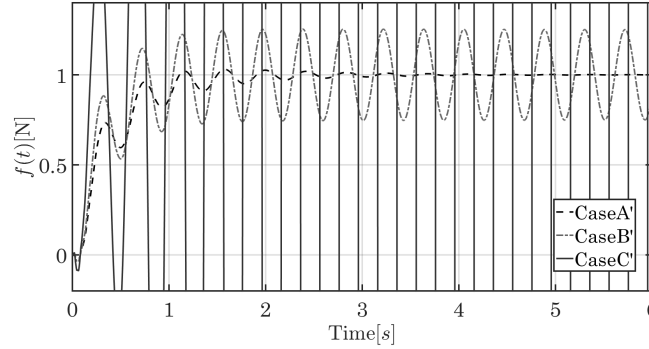
Figure 7: Contact-force $f(t)$ under the modified controller (48).

Next, we investigate the robustness of our controllers (9) and (48) with respect to uncertainty in physical parameters by simulation. In order to consider the situations that the bending rigidity EI is deviated by ΔEI during controller design, the value of EI in the controller is changed to $EI + \Delta EI$, where ΔEI is set as $0.5[\text{Nm}^2]$. Here, we compare our controllers (9) and (48) with the controller in the previous study [23]: the PD control of the strain at the root of the beam. That is, $u(t) = k_p(w_{xx}(0,t) - w_{xx}^d(0)) + k_d w_{xxt}(0,t)$. Here, note that the proposed controller is (9), the modified controller is (48), and the previous controller is the controller in [23].

The simulation result of the PD control of the root strain (the previous controller) is shown as a solid line in Fig. 8. Gains k_p and k_d are designed as $k_p = 4$ and $k_d = 2\sqrt{k_p}$. From this result, it can be confirmed that, when there is the measurement error of physical parameters such as EI, the target strain of $w_{xx}^d(0,t) = \frac{f_d L}{EI}$ designed in the previous controller is changed, so the contact-force $f(t)$ converges to a value different from the desired value. On the other hand, dashed line and dash-dotted line in Fig. 8 show the contact-force responses of the modified controller and proposed controller in section 4 and 3 when there is an error in the measured values of EI, respectively. Gains k_p and k_d in both controllers are set as $k_p =$(one fourth of the boundary value of the stable region) and $k_d = 2\sqrt{k_p}$. In other words, gains k_p and k_d in proposed controller are designed as $k_p = 2.23$ and $k_d = 2.99$ and gains in modified controller are designed as $k_p = 1.60$ and $k_d = 2.52$. From these lines in Fig. 8, we found that the responses of $f(t)$ converge to the designed value by our controllers (9) and (48), because the physical parameters are not used in the controllers.

In addition, we investigate the control performance in the case where ΔEI is doubled ($\Delta EI = 1.0[\text{Nm}^2]$) and the case where ΔEI is half ($\Delta EI = 0.25[\text{Nm}^2]$). Fig. 9 and 10 show the contact-force responses when $\Delta EI = 1.0$ and $\Delta EI = 0.25$, respectively. Here, note that the feedback gains and other parameters are the same as above. From these figures, we found that the responses of $f(t)$ converge to the desired value by our
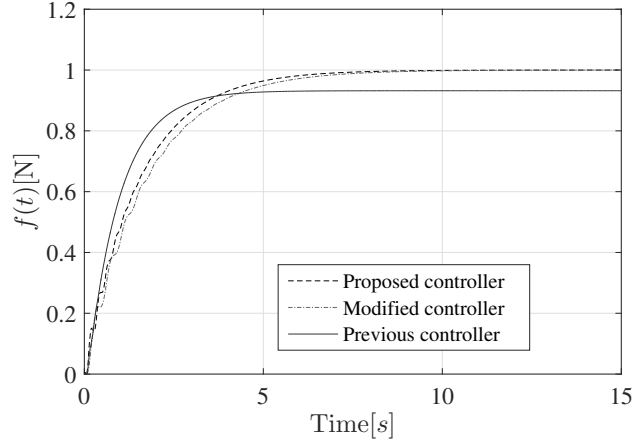
Figure 8: Cotact-force $f(t)$ when EI has uncertainty($\Delta EI = 0.5$).
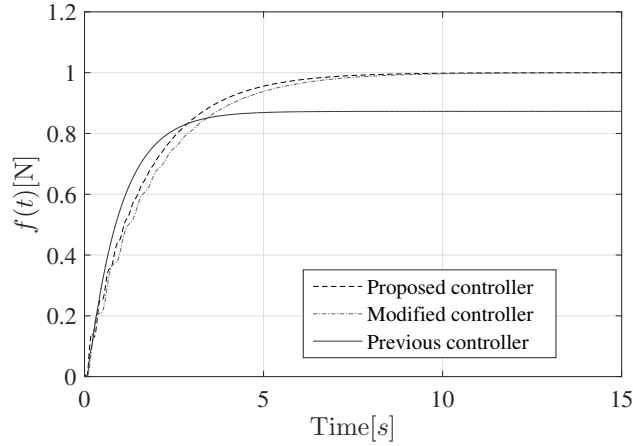
Figure 9: The contact-force $f(t)$ when EI deviates from the assumed value ($\Delta EI = 1.0$).

controllers even if ΔEI changes.

Finally, we investigate the disturbance responses of the proposed controller and modified controller. We add the following disturbance $d(t)$ to the control inputs from 15 [s] to 15.01 [s]:

$$d(t) = \left\{ \begin{array}{ll} 20 \ [\text{rad/s}^2] & \text{when } 15.00 \leq t \leq 15.005 \ [\text{s}] \\ -20 \ [\text{rad/s}^2] & \text{when } 15.005 \leq t \leq 15.01 \ [\text{s}] \end{array} \right.$$

The simulation results of the proposed controller are shown as light solid line in Fig. 11 and 12. Here, Fig. 11 shows the response of the contact-force and Fig. 12 shows the close-up of Fig. 11. Gains k_p and k_d of proposed controller are set as $k_p = 2.23$ and $k_d = 2.99$. On the other hand, the dark solid line in Fig. 11 and Fig. 12 show the simulation results of the modified controller. Gains k_p and k_d of the modified controller are set as $k_p = 1.60$ and $k_d = 2.52$ in order to make the stability of the modified controller becomes almost same as the stability of the proposed controller. From these lines in Fig. 11 and 12, it can be seen that the high-frequency vibration was excited by the disturbance, and the modified controller (48) suppress this high-frequency vibration than the proposed controller (9), and thus $f(t)$ converges to the designed value by the modified controller faster than by the proposed controller. From these points of view, we found that both controllers work well for the contact-force control of the flexible arm. Further, the modified controller

16
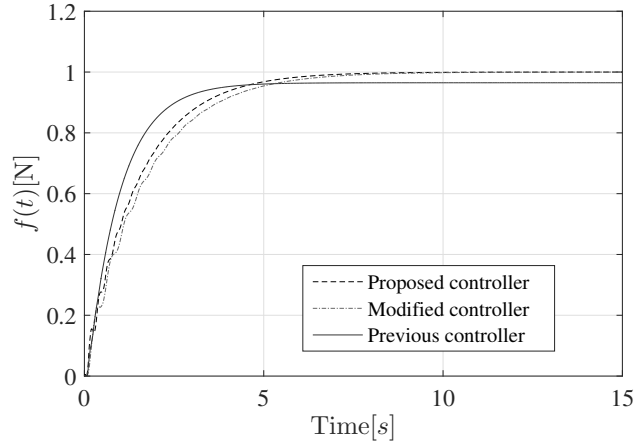
Figure 10: The contact-force $f(t)$ when EI deviates from the assumed value ($\Delta EI = 0.25$).
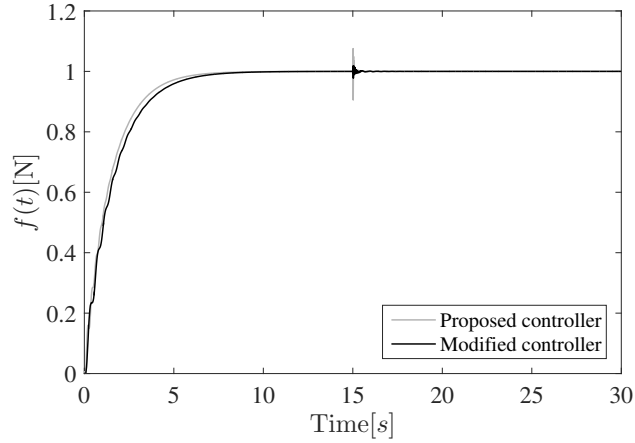
Figure 11: Contact-force $f(t)$ when adding impulse disturbance.

has higher performance than the proposed controller, but the stable region of the modified controller is narrower than the proposed controller.

6. Conclusion

In this paper, we discussed the contact-force control problem of a one-link flexible arm based on an infinite dimensional model. We proposed a boundary controller which consists of the feedback of the contact-force at the arm-tip and the time derivative of strain at the root of the arm without the need to use the physical parameters in the implementation of the controller. The closed-loop system is non-collocated, so there is a limit to the range of gain where the system becomes stable. Through the eigenvalue analysis, we proved that closed-loop system satisfies the spectrum-determined growth condition. Then, we showed that the closed-loop system becomes exponentially stable by setting feedback gains to place eigenvalues of the closed-loop system on the complex left half-plane. Further, we derived the range of the feedback gain that makes the system exponentially stable and confirmed the stable region by numerical simulation. On the other hand, to obtain high control performance, we proposed the modified controller which consists of the feedback of the contact-force and the time derivative of shear force at the root of the arm. Also, in this case, we
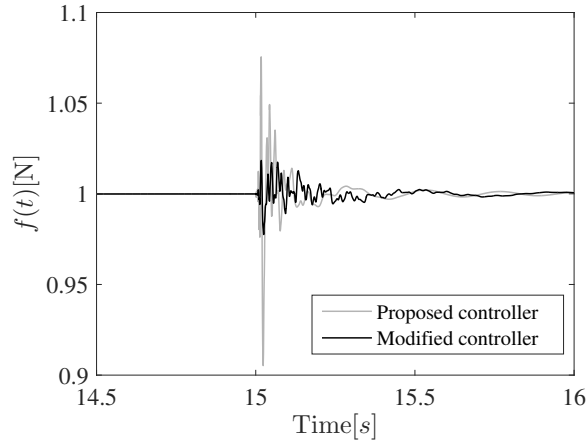
Figure 12: Contact-force $f(t)$ when adding impulse disturbance (Time=[14.5s 16s], $f(t)$=[0.9N 1.1N]).

analyzed the eigenvalue of the closed-loop system and obtained the range of the gain that makes the system exponentially stable and investigated the stable region by numerical simulation. In addition, we investigated the robustness to uncertainty in physical parameters. Although the stable region of the modified controller in section 4 is narrower than the stable region of the proposed controller in section 3, it is confirmed that the convergence speed of the modified controller is faster than the speed of the proposed controller when adding the disturbance to the control input and exciting the high-frequency vibrations.

As the next problem to be tackled is to investigate the stability of the system including the dynamics of the motor. Further, as future research, the results of this paper can be applied to cooperative control by multiple flexible arms and to cooperative transportation of space structure by flexible arms.

References

References

[1] L. Blanc, A. Delchambre, P. Lambert, Flexible Medical Devices : Review of Controllable Stiffness Solutions, Actuators (2017) 1–32.

[2] S. Robla-G, V. M. Becerra, J. R. Latta, E. González-S, C. Torre-F, J. Pérez-O, Working Together : A Review on Safe Human-Robot Collaboration in Industrial Environments, IEEE Access (2017) 26754–26773.

[3] S. Krishnan, L. Saggere, A multi-fingered micromechanism for coordinated micro/nano manipulation, Journal of Micromechanics and Microengineering 17 (3) (2007) 576–585.

[4] E. Radi, G. Bianchi, L. di Ruvo, Upper and lower bounds for the pull-in parameters of a micro- or nanocantilever on a flexible support, International Journal of Non-Linear Mechanics 92 (2017) 176–186.

[5] Z.-H. Luo, Direct strain feedback control of flexible robot arms: new theoretical and experimental results, IEEE Transactions on Automatic Control 38 (11) (1993) 1610–1622.

[6] M. A. Shubov, Asymptotics of aeroelastic modes and basis property of mode shapes for aircraft wing model, Journal of the Franklin Institute 338 (2) (2001) 171–185.

[7] B. Chentouf, J. M. Wang, Stabilization and optimal decay rate for a non-homogeneous rotating body-beam with dynamic boundary controls, J. Math. Anal. Appl. 318 (2) (2006) 667–691.

[8] A. Smyshlyaev, B. Guo, M. Krstic, Arbitrary decay rate for euler-bernoulli beam by backstepping boundary feedback, IEEE Transactions on Automatic Control 54 (5) (2009) 1134–1140.

[9] Ö. Morgül, On the strain feedback control of a flexible robot arm, in: Proc. of American Control Conference (ACC2011), 2011, pp. 1795–1800.

[10] L. Zhang, J. Liu, Adaptive boundary control for flexible two-link manipulator based on partial differential equation dynamic model, IET Control Theory and Applications 7 (1) (2013) 43–51.

[11] R. Curtain, H. Zwart, Stabilization of collocated systems by nonlinear boundary control, Systems & Control Letters 96 (2016) 11–14.

[12] W. He, S. Nie, T. Meng, Y.-J. Liu, Modeling and Vibration Control for a Moving Beam With Application in a Drilling Riser, IEEE Trans. Control Systems Technology 25 (3) (2017) 1036–1043.

18

[13] A. Tavasoli, Active disturbance rejection boundary control of Timoshenko beam with tip mass, ISA Transactions 80 (2018) 221 – 231.

[14] X. He, Z. Zhao, Y. Song, Active control for flexible mechanical systems with mixed deadzone-saturation input nonlinearities and output constraint, Journal of the Franklin Institute, In Press.

[15] T. Endo, F. Matsuno, Y. Jia, Boundary cooperative control by flexible timoshenko arms, Automatica 81 (2017) 377–389.

[16] T. Endo, M. Sasaki, F. Matsuno, Y. Jia, Contact-force control of a flexible timoshenko arm in rigid/soft environment, IEEE Trans. Autom. Control 62 (5) (2017) 2546–2553.

[17] S. Epponger, W. Seering, On dynamic models of robot force control, in: Proc. of the IEEE International Conference on Robotics and Automation (ICRA1986), 1986, pp. 29–34.

[18] B. Chiou, M. Shahinpoor, Dynamic stability analysis of a one-link force controlled flexible manipulator, Journal of Robotic Systems 5 (1988) 443–451.

[19] M. Madani, M. Moallem, Hybrid position/force control of a flexible parallel manipulator, Journal of the Franklin Institute 348 (6) (2011) 999–1012.

[20] F. Matsuno, S. Kasai, Modeling and robust force control of constrained one-link flexible arms, Journal of Robotic Systems 15 (8) (1998) 447–464.

[21] F. Matsuno, A. Hayashi, PDS cooperative control of two one-link flexible arms, in: Proc. of the IEEE International Conference on Robotics and Automation (ICRA2000), 2000, pp. 1490–1495.

[22] F. M. C. Ching, D. Wang, Exact solution and infinite-dimensional stability analysis of a single flexible link in collision, IEEE Trans. Robot. Autom 19 (6) (2003) 1015–1020.

[23] T. Endo, F. Matsuno, H. Kawasaki, Force control and exponential stabilisation of one-link flexible arm, Int. J. Control 87 (9) (2014) 1794–1807.

[24] W. He, Z. Jing, X. He, J.-k. Liu, C. Sun, Robust adaptive vibration control for a string with time-varying output constraint, Int J Robust Nonlinear Control 28 (2018) 5213–5231.

[25] Y. Zhu, M. Krstic, H. Su, Adaptive global stabilization of uncertain multi-input linear time-delay systems by pde full-state feedback, Automatica 96 (2018) 270–279.

[26] Y. Cao, D. Cao, W. Huang, Dynamic modeling and vibration control for a t-shaped bending and torsion structure, International Journal of Mechanical Sciences 157-158 (2019) 773–786.

[27] Z. Lin, S. Lin, S. Wu, Z. Liang, Vibration control of a flexible spacecraft system with input backlash, IEEE Access 7 (2019) 87017–87026.

[28] Y. Zhang, X. Guan, Active damping control of flexible appendages for spacecraft, Aerospace Science and Technology 75 (2018) 237–244.

[29] Q. Hu, G. Ma, Vibration suppression of flexible spacecraft during attitude maneuvers, Journal of Guidance, Control, and Dynamics 28 (2) (2005) 377–380.

[30] A. Arisoy, M. Gökasan, O. S. Bogosyan, Tip position control of a flexible-link arm, in: Proc. of 9th IEEE International Workshop on Advanced Motion Control, 2006, pp. 445–450.

[31] B.-Z. Guo, W. Guo, The strong stabilization of a one-dimensional wave equation by non-collocated dynamic boundary feedback control, Automatica 45 (3) (2009) 790–797.

[32] Z.-J. Han, G.-Q. Xu, Dynamical behavior of a hybrid system of nonhomogeneous timoshenko beam with partial non-collocated inputs, Journal of Dynamical and Control Systems 17 (1) (2011) 77–121.

[33] Y. L. Chen, G. Q. Xu, Exponential stability of uniform Euler-Bernoulli beams with non-collocated boundary controllers, Journal of Mathematical Analysis and Applications 409 (2) (2014) 851–867.

[34] L.-Y. Liu, H.-C. Lin, Tip-contact force control of a single-link flexible arm using feedback and parallel compensation approach, Robotica 31 (5) (2013) 825–835.

[35] K. Yamaguchi, T. Endo, Y. Kawai, F. Matsuno, Contact-force control of one-link flexible arm without using physical parameters in the controller design, in: Proc. of 12th France-Japan and 10th Europe-Asia Congress on Mechatronics, 2018, pp. 195–200.

[36] A. Pazy, Semigroups of linear operators and applications to partial differential equations, Springer-Verlag, 1983.

[37] T. Kato, Perturbation Theory for Linear Operators, Springer Science and Business Media, 1995.

[38] Z. H. Luo, B. Z. Guo, Ö. Morgül, Stability and Stabilization of Infinite Dimensional Systems with Applications, Springer-Verlag, 1999.

[39] B. Z. Guo, J. M. Wang, Riesz basis generation of abstract second-order partial differential equation systems with general non-separated boundary conditions, Numerical Functional Analysis and Optimization 27 (3-4) (2006) 291–328.

[40] J. Ackermann, Robust Control: Systems with Uncertain Physical Parameters, Springer-Verlag London, 1993.

[41] N. Yamaguchi, H. Kanoh, Design of robust PID parameters for distributed parameter processes, in: Proc. of IFAC Computer Aided Control Systems Design, 2000, pp. 221–226.

[42] Z. H. Luo, B. Z. Guo, Shear force feedback control of a single-link flexible robot with a revolute joint, IEEE Transactions on Automatic Control 42 (1) (1997) 53–65.

[43] B.-Z. Guo, J.-M. Wang, S.-P. Yung, On the c_0-semigroup generation and exponential stability resulting from a shear force feedback on a rotating beam, Systems & Control Letters 54 (6) (2005) 557–574.